





**Magnetic field induced Weyl state in the van der Waals–type antiferromagnet GdTe<sub>3</sub>**Y. M. Wan <sup>1,\*</sup> E.-J. Cheng<sup>2,3,\*</sup> H.-Y. Ma<sup>4,5,\*</sup> X. F. Yang<sup>1,\*</sup> X. F. Hou <sup>4</sup> X. J. Chen<sup>6</sup> X. Zhang<sup>1</sup> C. Y. Xi,<sup>7</sup>  
Z. C. Zhong<sup>6,8</sup> J. P. Liu <sup>4,5</sup> Y. F. Guo<sup>4,‡</sup> and S. Y. Li <sup>1,9,10,§</sup><sup>1</sup>State Key Laboratory of Surface Physics, Department of Physics, Fudan University, Shanghai 200433, China<sup>2</sup>Leibniz Institute for Solid State and Materials Research (IFW-Dresden), Dresden 01069, Germany<sup>3</sup>Max Planck Institute for Chemical Physics of Solids, Dresden 01187, Germany<sup>4</sup>School of Physical Science and Technology, ShanghaiTech University, Shanghai 201210, China<sup>5</sup>ShanghaiTech Laboratory for Topological Physics, ShanghaiTech University, Shanghai 201210, China<sup>6</sup>CAS Key Laboratory of Magnetic Materials and Devices, Zhejiang Province Key Laboratory of Magnetic Materials and Application Technology, Ningbo Institute of Materials Technology and Engineering, Chinese Academy of Sciences, Ningbo 315201, China<sup>7</sup>Anhui Province Key Laboratory of Condensed Matter Physics at Extreme Conditions, High Magnetic Field Laboratory of the Chinese Academy of Sciences, Hefei 230031, China<sup>8</sup>China Center of Materials Science and Optoelectronics Engineering, University of Chinese Academy of Sciences, Beijing, 100049, China<sup>9</sup>Collaborative Innovation Center of Advanced Microstructures, Nanjing 210093, China<sup>10</sup>Shanghai Research Center for Quantum Sciences, Shanghai 201315, China

(Received 6 January 2023; revised 12 September 2023; accepted 30 October 2023; published 15 November 2023)

GdTe<sub>3</sub>, a van der Waals–type antiferromagnetic (AFM) metal with high mobility, is gaining a lot of attention for its potential use in high-speed spintronic devices as well as for fundamental physics research. Due to the magnetocrystalline anisotropy of GdTe<sub>3</sub>, exotic effects are envisaged, when the magnetic configurations interact with an external magnetic field. In this work, a magnetic-field-induced Weyl state in GdTe<sub>3</sub> is revealed. In the AFM state, GdTe<sub>3</sub> is topologically trivial. However, when an external magnetic field exceeding  $\sim 20$  T aligns all spins, band splitting occurs, and then a topological transition is induced, i.e., from a trivial metallic state to a topological Weyl metallic state. In addition, a topological change of Fermi surfaces, i.e., a field-induced Lifshitz transition, is uncovered, which may also be rooted in band splitting. Moreover, high-pressure electrical transport measurements reveal a peculiar superconducting transition with a nearly invariant superconducting transition temperature ( $T_c \sim 4.2$  K) spanning a wide range of pressure up to 48 GPa. These findings imply that GdTe<sub>3</sub> provides a unique platform for investigating not only the interactions of charge-density-wave fluctuations and superconductivity but also the interplay between magnetism and topology.

DOI: [10.1103/PhysRevB.108.205132](https://doi.org/10.1103/PhysRevB.108.205132)**I. INTRODUCTION**

In recent decades, magnetic van der Waals (vdW) type materials have attracted a great deal of interest due to various intriguing electronic, magnetic, and optical properties [1–14], such as giant tunneling magnetoresistance [7–10], tunable magnetism [11–13], giant nonreciprocal second-harmonic generation [14], etc. Thanks to the layered structure with weak vdW force in the interlayers, magnetic vdW-type materials can be mechanically exfoliated into monolayer or few-layer flakes, which paves the way for the realization of twistrionic or high-speed spintronic devices [15–17]. Moreover, due to the existence of charge-density-wave (CDW) instabilities, the phase diagrams of magnetic vdW-type materials are enriched, and the additional electronic degree of freedom offers an alternative approach for exploring the underlying physics of the interactions between CDW, superconductivity, and magnetism [18].

For magnetic materials, another interesting subject is exploring novel topological states [19,20]. When magnetic elements are included, the time-reversal (TR) symmetry is broken, resulting in various exotic phenomena, for example, anomalous Hall/Nernst effects [21–23], topological Hall effect [24,25], and topological magnetic textures (for example, skyrmions) [26]. More interestingly, the coupling of magnetic configurations with the electronic wave functions leads to extraordinary topological states, such as a spin-fluctuation-induced Weyl semimetal state in EuCd<sub>2</sub>As<sub>2</sub> [27], a magnetism-induced topological transition in EuAs<sub>3</sub> [28], a magnetic-exchange-induced Weyl state in EuCd<sub>2</sub>Sb<sub>2</sub> [29], magnetization tunable Weyl states in EuB<sub>6</sub> [30], a magnetic-field-induced ideal type-II Weyl state in Mn(Bi<sub>1-x</sub>Sb<sub>x</sub>)<sub>2</sub>Te<sub>4</sub> [31], and a Weyl-mediated magnetism in NdAlSi [32]. The relationship between magnetism and topology is still tricky, despite notable advancements in magnetic topological materials (MTMs). Furthermore, most MTMs are three dimensional (3D), thus vdW conductive magnetic materials are rare and they are expected to exhibit exotic properties with potential use in spintronic devices.

Recently, the magnetic vdW-type RTe<sub>3</sub> family ( $R$  = rare earth) with CDW instability has attracted increasing attention

\*These authors contributed equally to this work.

†erjian\_cheng@163.com

‡guoyf@shanghaitech.edu.cn

§shiyian\_li@fudan.edu.cn

[33–45], among which GdTe<sub>3</sub> stands out for several surprising properties, such as the slow oscillations of intralayer magnetoresistance (MR) [46], pressure-induced superconductivity [43], high mobility beyond 60 000 cm<sup>2</sup> V<sup>-1</sup> s<sup>-1</sup> comparable to black phosphorus [47], the observation of axial Higgs mode [48], robust CDW and stripe antiferromagnetic order at the two-dimensional (2D) limit [49], and field-induced novel magnetic behavior [50]. Nevertheless, the topological properties in GdTe<sub>3</sub> are heretofore uninvestigated.

In this paper, we demonstrate that external magnetic field fully polarizes the spins above  $\sim 20$  T, and then the induced band splitting leads to a topological transition from a topologically trivial metallic state in the AFM state to a topological Weyl metallic state in the ferromagnetic state. Besides, a field-induced Lifshitz transition is also revealed. The superconducting transition is also investigated under higher pressure, and displays a broad pressure dependence with an invariant superconducting transition temperature ( $T_c$ ) of  $\sim 4.2$  K up to 48 GPa, the highest pressure we measured. These findings imply that magnetic vdW-type GdTe<sub>3</sub> offers a special platform for studying the relationships between CDW, superconductivity, magnetism, and topology.

## II. EXPERIMENTAL DETAILS

GdTe<sub>3</sub> single crystals were synthesized through a self-flux method, as described in Ref. [37]. The large natural surface is identified to be the (010) plane by a D8 Advance x-ray diffractometer from Bruker. For electrical transport measurements, one typical GdTe<sub>3</sub> single crystal was cut into a bar shape. A standard four-probe method was used for the longitudinal resistance measurements. Data were collected in a <sup>3</sup>He cryostat. High-field measurements were performed at the Steady High Magnetic Field Facilities (SHMFF) in Hefei. High-pressure transport measurements were performed in a physical property measurement system (PPMS, Quantum Design) by using a diamond anvil cell (DAC). Pressure was determined by the pressure-induced fluorescence shift of ruby before and after measurements at room temperature [51].

First-principles calculations based on density functional theory (DFT) are performed using the Vienna *Ab initio* Simulation Package (VASP) which adopts the projector-augmented wave method [52,53]. The lattice constants of the fully relaxed structure are  $a = 4.273$  Å,  $b = 25.367$  Å, and  $c = 4.322$  Å. The energy cutoff is set at 400 eV and the exchange-correlation functional of Perdew-Burke-Ernzerhof (PBE) type is used for the electronic band calculations [54,55]. For the lattice relaxation, vdW corrections of the DFT-D3 methods are adopted in consideration of the vdW interactions between the layers [56]. The convergence criteria for the total energy and forces are set to 10<sup>-6</sup> eV and  $\sim 0.001$  eV/Å, respectively. The Brillouin zone (BZ) is sampled by a  $\Gamma$ -centered  $8 \times 8 \times 24$  **k** mesh for the primitive structure. The Wannier tight-binding models used for the topological calculations are obtained through the WANNIER90 code [57–60].

## III. RESULTS AND DISCUSSION

GdTe<sub>3</sub> crystallizes in an orthorhombic structure with space group *Bmmb* [or in its standard setting *Cmcm* (No. 63)] [37,47,48,50]. Note that the definitions of crystallographic

axis for the space groups *Bmmb* and *Cmcm* are different. Here, we adopt the standard setting *Cmcm*, and therefore GdTe<sub>3</sub> consists of double Te square-net sheets and corrugated GdTe slabs stacking along the long crystal *b* axis [Fig. 1(a)]. To shed light on the topological properties, the electronic band structure is calculated. Figure 1(c) exhibits the band structure with spin-orbit coupling (SOC) of GdTe<sub>3</sub> in the AFM state. Some bands intersect the Fermi level, suggesting that GdTe<sub>3</sub> is a good metal. However, if a curved chemical potential between conduction and valence bands is defined [marked in red in Fig. 1(c)], a trivial gap traverses the entire BZ [61–63]. In other words, GdTe<sub>3</sub> in the AFM state is topologically trivial.

Given that the spins in the AFM state can be aligned by an external magnetic field, it would be interesting to investigate how the band structure evolves in the fully spin-polarized state. Figure 1(d) shows the calculated band structure with SOC for the ferromagnetic state with spins aligned along *b* axis. The total energy of the ferromagnetic state is only  $\sim 3$  meV higher than the AFM state, implying that an external magnetic field could serve as an effective knob to tune the ground state. With magnetic field tuning, the linear bands around the Fermi energy remain nearly unchanged. This is because Te atoms are the source of the linear bands surrounding the Fermi energy, and magnetic field tuning has little impact on them. However, below 0.2 eV, the *d* orbitals of Gd atoms start to contribute. The external magnetic field reduces the spin degeneracy, and then results in band splitting, which is indeed observed in the band calculations [Fig. 1(d)]. In the gap between valence and conduction bands, several Weyl nodes appear, but not at the high-symmetry points or along high-symmetry lines. The inset of Fig. 1(d) shows one representative Weyl node along a non-high-symmetry line. There are 20 pairs of Weyl nodes in the BZ, and two of them closest to  $E_F$  are displayed in Table I. In addition to the topological transition, the topological change of Fermi surfaces is clearly evident, as shown in the insets of Figs. 1(e) and 1(f). Putting together the results, we propose that GdTe<sub>3</sub> is a topological Weyl metal in the magnetic-field-induced ferromagnetic state, and the band splitting gives rise to a Lifshitz transition.

To verify the topological property, electrical transport was implemented. Figure 2(a) shows the longitudinal resistivity of GdTe<sub>3</sub> in zero field. The CDW transition with a transition temperature of  $\sim 376$  K is evident, consistent with previous reports [37,43,47]. The inset of Fig. 2(a) shows the x-ray diffraction (XRD) pattern on the largest natural surface of a typical GdTe<sub>3</sub> single crystal, demonstrating that the largest flat plane is the *ac* plane corresponding to the *Cmcm* setting [37]. For GdTe<sub>3</sub>, there are two AFM transitions, at 11.5 K ( $T_{N1}$ ) and 9.5 K ( $T_{N2}$ ), but the latter is hardly recognized in magnetization profiles [the inset of Fig. 2(b)]. Besides, there exists an anomaly at 7 K ( $T_1$ ) that might arise from the incommensurate CDW state [47,50]. In order to ascertain the critical magnetic field required for the suppression of antiferromagnetic order, field dependence of the magnetic transitions is plotted, as shown in Fig. 2(b). By assuming a quadratic field dependence, two critical magnetic fields of  $\sim 20$  and  $\sim 13.7$  T for  $T_{N1}$  and  $T_1$ , respectively, are estimated. Figure 2(c) shows the longitudinal ( $\rho_{xx}$ ) and transverse ( $\rho_{yx}$ ) resistivities at 2 K. Figure 2(d) is the calculated Hall conductivity. A fit to the data using

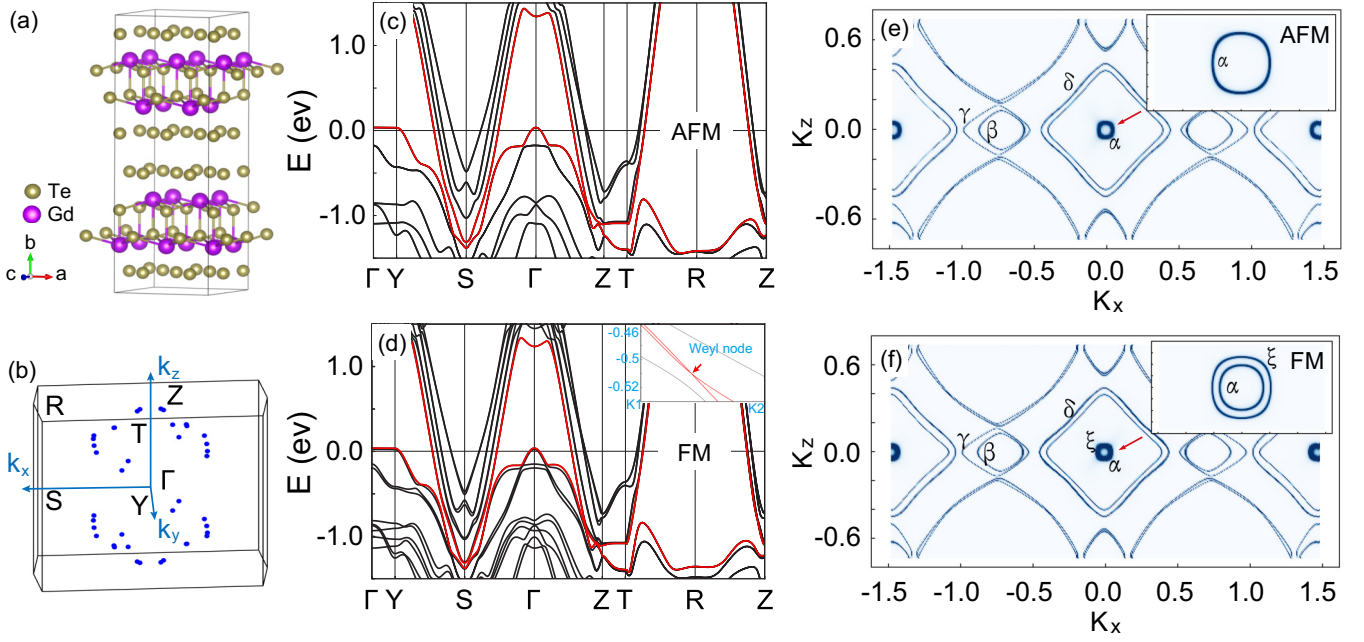


FIG. 1. (a) Schematic crystal structure for the orthorhombic  $\text{GdTe}_3$  (Gd: purple; Te: yellow) with space group  $Cmcm$  (No. 63). Double Te square-net sheets and corrugated GdTe slabs stack along the  $b$  axis. (b) Three-dimensional (3D) Brillouin zone (BZ). There are 20 pairs of Weyl nodes in the BZ. Electronic band structures of  $\text{GdTe}_3$  in (c) the antiferromagnetic state and (d) the field-driven ferromagnetic state with spin-orbit coupling (SOC) considered. If a curved chemical potential between conduction and valence bands (marked in red) is defined, there is a trivial gap traversing through the BZ for the antiferromagnetic state, while several crossing points (i.e., Weyl nodes) exist for the ferromagnetic state. The inset shows one representative Weyl node along a non-high-symmetry line. (e) and (f) Constant energy mappings taken at  $E = 0$  eV for the antiferromagnetic and ferromagnetic states, respectively. Insets depict a zoomed-in view centered around the  $\Gamma$  point, from which a field-induced new pocket, i.e.,  $\xi$  can be resolved.

a two-band model yields  $n_e = 1.93(4) \times 10^{18} \text{ cm}^{-3}$ ,  $n_h = 1.547(4) \times 10^{20} \text{ cm}^{-3}$ ,  $\mu_e = 1.83(4) \times 10^4 \text{ cm}^2 \text{ V}^{-1} \text{ s}^{-1}$ , and  $\mu_h = 1.401(4) \times 10^3 \text{ cm}^2 \text{ V}^{-1} \text{ s}^{-1}$  for electron density, hole density, electron mobility, and hole mobility, respectively. The extracted mobility is in the same order of magnitude as reported [47], verifying the high-mobility feature of  $\text{GdTe}_3$ . The electron density and hole density are two and one orders of magnitude lower than in previous reports, respectively. Our sample is therefore hole doped, implying that the position of the Weyl nodes with respect to  $E_F$  should be less than 0.52 eV. The precise impact of Weyl node position on transport properties varies in different systems, so the extent to which the position of Weyl nodes affects transport properties in  $\text{GdTe}_3$  remains to be further explored.

Figure 3(a) presents the high-field magnetoresistance with magnetic field applied along  $b$  axis at several selected temperatures, and distinct Shubnikov–de Haas (SdH) oscillations are visible. The SdH oscillation amplitudes could be described by

TABLE I. The location of two pairs of Weyl nodes in the field-driven ferromagnetic state of  $\text{GdTe}_3$ .

$(k_x, k_y, k_z)$	$E$ (eV)
$(-0.19701, -0.22057, 0.27348)$	-0.52
$(0.19701, 0.22057, -0.27349)$	-0.52003
$(0.19686, 0.22066, 0.27379)$	-0.52099
$(-0.19686, -0.22066, -0.27379)$	-0.52101

the Lifshitz-Kosevich formula [28,61,64],

$$\Delta\rho \propto \frac{2\pi^2 k_B T / \hbar\omega_c}{\sinh(2\pi^2 k_B T / \hbar\omega_c)} e^{-\frac{2\pi^2 k_B T_D}{\hbar\omega_c}} \cos 2\pi \left( \frac{F}{B} - \gamma - \delta \right),$$

where  $\omega_c = eB/m^*$  and  $T_D$  represent the cyclotron frequency and Dingle temperature, respectively. The Berry phase  $2\pi\beta$  will be discussed later.  $\gamma = 1/2 - \phi_B/2\pi$  represents the Onsager phase factor with the Berry phase  $\phi_B$ . The phase shift  $\delta$  is 0 or  $\pm 1/8$  for a quasi-2D or a corrugated 3D Fermi surface, respectively. The cyclotron effective mass  $m^*$  can be deduced from the thermal damping factor  $R_T = 2\pi^2 k_B T / \hbar\omega_c / \sinh(2\pi^2 k_B T / \hbar\omega_c)$ . The average magnetic field  $B$  in the formula is determined from  $1/B = (1/B_1 + 1/B_2)/2$ , where  $B_1$  and  $B_2$  are the minimum and maximum values of the field range of the oscillations.

To reveal the evolution of Fermi surfaces in the ferromagnetic state, we analyze the oscillations in the range of 25–38 T. Figure 3(b) depicts the fast Fourier transform (FFT) analysis for the oscillatory components at 0.3 K. Four oscillation frequencies, i.e., 65, 301, 501, and 803 T, are distinguished, and are assigned to  $\alpha$ ,  $2\xi$  (discuss later),  $\beta$ , and  $\gamma$  bands, respectively. Previously, multiple frequencies from quantum oscillations have been reported [47], i.e., 60 T ( $\alpha$ ), 472 T ( $\beta_1$ ), 506 T ( $\beta_2$ ), 813 T ( $\gamma_1$ ), 847 T ( $\gamma_2$ ), 2230 T ( $\eta$ ), 3708 T ( $\delta_1$ ), and 3948 T ( $\delta_2$ ). Here, from SdH oscillations, the  $\beta_1$  and  $\beta_2$  frequencies cannot be distinguished, and the  $\gamma_1$  and  $\gamma_2$  bands frequencies cannot be resolved either due to the broad peak. Besides, the high frequencies for  $\eta$ ,  $\delta_1$ , and  $\delta_2$  cannot be resolved in our experiments. Beyond that, the main frequencies are

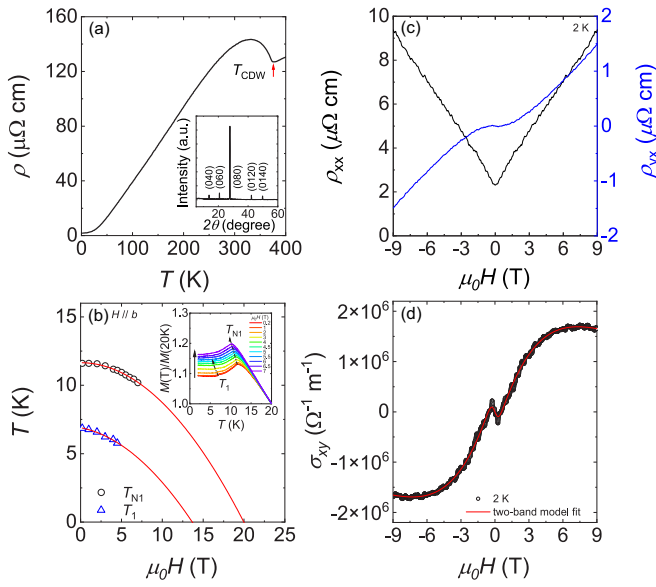


FIG. 2. (a) Temperature-dependent resistivity of GdTe<sub>3</sub> single crystal in zero magnetic field. A distinct charge-density-wave (CDW) transition with a critical transition temperature ( $T_{\text{CDW}}$ ) of  $\sim 376$  K is evident. The inset shows the x-ray diffraction (XRD) pattern on the largest natural surface of a typical as-grown GdTe<sub>3</sub> single crystal, demonstrating that the largest flat plane is the  $ac$  plane. (b) Magnetic field dependence of the antiferromagnetic transition temperature ( $T_{N1}$ ) and the anomalous transition temperature ( $T_1$ ) that possibly originates from the incommensurate CDW state. By assuming a quadratic field dependence, two critical magnetic fields of  $\sim 20$  and  $\sim 13.7$  T for  $T_{N1}$  and  $T_1$ , respectively, are estimated. The inset displays the magnetization normalized to that at 20 K at several selected fields. (c) Longitudinal ( $\rho_{xx}$ ) and transverse ( $\rho_{yx}$ ) resistivities at 2 K. (d) Hall conductivity ( $\sigma_{xy}$ ) at 2 K. The red line represents the fit to the data by using a two-band model, i.e.,  $\sigma_{xy}(B) = eB\{n_h\mu_h^2/[1 + (\mu_h^2B^2)] - n_e\mu_e^2/[1 + (\mu_e^2B^2)]\}$ .

overall consistent with the previous reports [47]. Strikingly, the emerged  $\xi$  band with a frequency of 301 T has not been reported before, even in the nonmagnetic analog LaTe<sub>3</sub> [65], indicating its unusual origin.

To figure out the origin of the  $\xi$  frequency, we calculated the oscillatory frequencies. The calculated frequencies in the FM state at  $E_F \sim -0.01$  eV give  $\sim 75$  T from band 27 for the  $\alpha$  band;  $\sim 130$  T from band 28 for  $\xi$ ;  $\sim 347$ ,  $\sim 530$ ,  $\sim 565$ , and  $\sim 655$  T from bands 35–36 for  $\beta$ ;  $\sim 754$ ,  $\sim 890$ ,  $\sim 956$ , and  $\sim 1000$  T from bands 33–34 for  $\gamma$ ;  $\sim 3400$  and  $\sim 3680$  T from bands 29–30 for  $\delta$ . In the AFM state, most frequencies are consistent with those in the FM state, except that the frequency of  $\sim 130$  T cannot be found. As displayed in Fig. 3(b), due to the broad peak of  $\alpha$ , the  $\xi$  cannot be resolved. However, its second harmonic frequency  $\sim 260$  T is nearly consistent with our experimental value  $\sim (301 \pm 40)$  T. By fitting the temperature dependence of the thermal damping factor  $R_T$ , the cyclotron effective mass  $m^*$  for the  $2\xi$  band is extracted [Fig. 3(c)], yielding  $0.17(1)m_0$ . The Dingle temperature ( $T_D$ ) is also calculated to be  $\sim 42.4$  K, as shown in the inset of Fig. 3(c). According to the LK equation,  $T_D = \hbar/2\pi k_B\tau_Q$ , where  $\hbar$ ,  $k_B$ , and  $\tau_Q$  are the reduced Planck constant, the Boltzmann constant, and the quantum scattering lifetime,

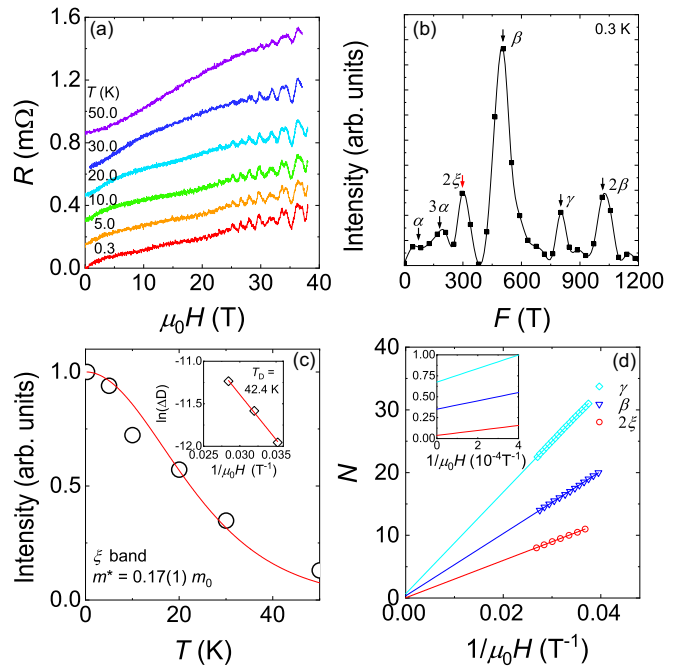


FIG. 3. (a) Shubnikov–de Haas (SdH) oscillations in GdTe<sub>3</sub> at several temperatures. The profiles are vertically shifted with an offset of 0.15 mΩ for clarity. (b) Fast Fourier transform (FFT) analysis for the oscillatory components of resistance above 25 T, identifying five frequencies, i.e., 65, 301, 501, and 803 T, which are assigned to  $\alpha$ ,  $2\xi$ ,  $\beta$ , and  $\gamma$ , respectively. (c) Temperature dependence of the normalized FFT amplitude at 0.3 K. The solid line shows the fit to the Lifshitz-Kosevich (LK) formula for the  $2\xi$  band. The inset shows the LK fit to the oscillatory component of resistance for  $2\xi$  band to extract the Dingle temperature ( $T_D$ ).  $\Delta D$  is defined to be  $\Delta D = \Delta\rho/R_T$  with  $R_T$  the thermal damping factor. By plotting  $\ln(\Delta D)$  vs  $1/\mu_0H$ ,  $T_D$  can be obtained through a linear fit. (d) Landau level index  $N$  plotted against  $1/\mu_0H$  for the  $2\xi$ ,  $\beta$ , and  $\gamma$  bands. Lines represent linear fits. The inset shows the extrapolation of  $1/\mu_0H$  to zero.

respectively. Therefore, the quantum scattering lifetime  $\tau_Q$  is estimated to be  $2.9 \times 10^{-14}$  s. Furthermore, the quantum mobility  $\mu_Q = e\tau_Q/m^*$  is obtained to be  $\sim 300$  cm<sup>2</sup>/Vs.

Now we turn to the topological property of GdTe<sub>3</sub>. Figure 3(d) shows the Landau level index  $N$  fan diagram for  $2\xi$ ,  $\beta$ , and  $\gamma$  bands. Due to the weak signal of  $\alpha$ , the plot for  $\alpha$  is not shown. Here, we assign integer indices to the peak positions and half integer indices to the valley positions in  $(\mu_0H)^{-1}$ . The data fall into very straight lines, and the linear fits give the intercepts  $0.04 \pm 0.07$ ,  $0.35 \pm 0.12$ , and  $0.67 \pm 0.08$  for  $2\xi$ ,  $\beta$ , and  $\gamma$  bands, respectively. As mentioned, the intercept falling between  $3/8$  and  $5/8$  suggests trivial band topology, while the intercept in the range of  $-1/8$  to  $1/8$  indicates nontrivial topology [28,61,64]. Therefore, these results provide a strong hint that GdTe<sub>3</sub> in the ferromagnetic state possesses nontrivial topology.

In quantum materials, pressure—as a clean and effective approach for tuning the crystal structure associated with the reconstruction of Fermi surfaces and the interplay among multiple degrees of freedom—plays a significant role [66], in particular for exploring the interplay between CDW and

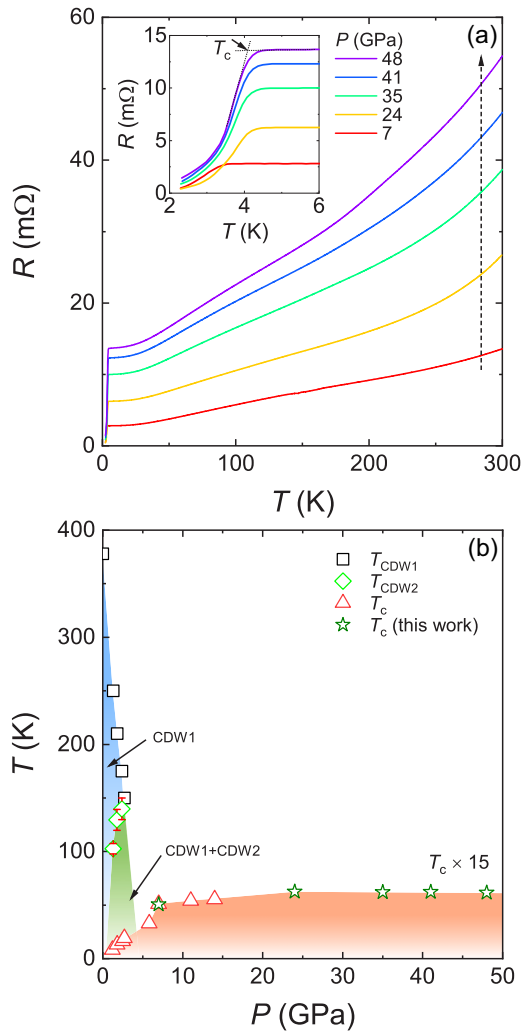


FIG. 4. (a) Temperature dependence of resistance for GdTe<sub>3</sub> under various pressures. The inset shows the superconducting transitions at low temperature. The superconducting transition temperature ( $T_c$ ) is defined as depicted in the picture. (b) Temperature vs pressure phase diagram for GdTe<sub>3</sub>. CDW1 and CDW2 denote two charge-density-wave (CDW) regimes. The values of CDW transition temperature and the superconducting transition temperature under low pressure are taken from Ref. [43]. Above  $\sim 24$  GPa,  $T_c$  is nearly invariant up to 48 GPa, the highest pressure we measured.

superconductivity. Previously, the pressure technique has been implemented in GdTe<sub>3</sub> and its siblings  $R\text{Te}_3$  ( $R = \text{La, Ce, Pr, Nd, Sm, Tb, Dy}$ ), finding the suppression of CDW under pressure [39–43]. In addition, superconductivity has been induced in GdTe<sub>3</sub>, TbTe<sub>3</sub>, and DyTe<sub>3</sub> [43]. Among the  $R\text{Te}_3$  family, there are three types of CDW transitions [45,67,68]. The first CDW arises from the Te-Te planes below the transition temperature  $T_{\text{CDW}1}$  with an incommensurate wave vector  $q_1 = (0, 0, \sim 2/7c^*)$  [69,70]. With heavier rare earth elements, a second CDW below a lower transition temperature  $T_{\text{CDW}2}$  forms with wave vector  $q_2 = (\sim 1/3a^*, 0, 0)$  [67,71,72]. With further reducing temperature, a third CDW develops, possibly coming from a lifting of the degeneracy of conduction bands of double Te net sheets, which is derived from optical conductivity experiments [45,67,68]. In

$R\text{Te}_3$ , the Fermi surface nesting and the electron-phonon coupling play important roles in driving the formation of CDWs [36,73]. For GdTe<sub>3</sub>, with increasing pressure, the first CDW transition ( $T_{\text{CDW}1}$ ) declines, while the second CDW transition ( $T_{\text{CDW}2}$ ) increases, and converges with  $T_{\text{CDW}1}$  at an intermediate pressure, as proposed by Zocco *et al.* [43]. Under low pressure, a domelike pressure phase diagram is proposed [43]. At 1.2 GPa, the superconductivity with a critical temperature  $T_c$  of 0.55 K arises, and then the  $T_c$  increases to  $\sim 1.3$  K at 2.7 GPa [43]. In contrast to the decline of overall CDW transition, the increase of  $T_c$  implies the competition between the CDW and superconductivity [43]. Beyond 2.7 GPa,  $T_c$  shows a steep enhancement at  $\sim 6$  GPa [43]. However, such an enhancement coming from tellurium inclusions cannot be completely excluded [43]. Therefore, higher pressure is needed.

Figure 4(a) shows the temperature dependence of resistance for GdTe<sub>3</sub> under various pressures. At 7 GPa,  $T_c$  is 3.4 K, which is consistent with a previous report [43]. Increasing pressure to 24 GPa,  $T_c$  is further enhanced to  $\sim 4.2$  K. Then  $T_c$  remains nearly invariable up to 48 GPa, the highest pressure we measured. For tellurium, pressure could induce multiple structural phase transitions accompanied by the presence of superconductivity [74,75].  $T_c$  in pressurized tellurium peaks at  $\sim 6.3$  GPa with a maximum value of  $\sim 4.3$  K, and then decreases to  $\sim 2.5$  K with pressure increasing to  $\sim 30$  GPa [75]. Above  $\sim 30$  GPa,  $T_c$  is significantly enhanced to  $\sim 8$  K, which corresponds to the structural phase transition from the  $\beta$ -Po type to the body-centered cubic (bcc) type, and then it monotonically decreases with pressure [75]. At 35 and 42 GPa, the  $T_c$ 's for tellurium are 7.4 and 4.5 K, respectively [75]. Therefore, the pressure evolution of  $T_c$  observed in GdTe<sub>3</sub> is different from tellurium, excluding the extrinsic superconductivity from tellurium inclusions.

We plot the pressure phase diagram of GdTe<sub>3</sub> in Fig. 4(b), and the CDW transition temperatures and the  $T_c$  from a previous study are also added [43]. The superconducting transition displays an anomaly at  $\sim 5$  GPa. Zocco *et al.* argued that there is a domelike region for GdTe<sub>3</sub> under low pressure (below 5 GPa) [43]. If this is the case, the superconductivity beyond 5 GPa is supposed to derive from a second superconducting state. For magnetic systems, two superconducting states are often observed, usually associated with unconventional superconductivity [76]. The origin of the second superconducting state has two scenarios. The first is that the superconductivity arises from the pressure-tuning fluctuations of magnetic ordering. However, the weak anomaly in resistivity for the AFM ordering makes it difficult for us to determine how the AFM ordering evolves with pressure [43]. Alternatively, the superconductivity may come from a structural phase transition induced by pressure. In CeTe<sub>3</sub>, high-pressure XRD experiments demonstrated that the slight orthorhombic distortion at ambient pressure is suppressed with increasing pressure [40]. GdTe<sub>3</sub> shares the same crystal structure with CeTe<sub>3</sub>, and therefore pressure is presumed to have an important effect on the structural evolution. To elaborate whether the superconductivity arises from magnetic fluctuations or a structural phase transition, more experiments, for example, high-pressure magnetization, heat capacity, and XRD measurements are called for.

Besides, it was proposed that the Fermi surface nesting and the electron-phonon coupling play crucial roles in the  $R\text{Te}_3$  family [77–80]. Therefore, in addition to the scenarios mentioned above, pressure may modify the crystal structure of  $\text{GdTe}_3$ , and consequently tune the Fermi surface nesting and the strength of electron-phonon coupling, leading to the steep enhancement of  $T_c$  [81]. We note that a nearly invariant  $T_c$  is also found in some topological systems, such as  $\text{Cd}_3\text{As}_2$  [82],  $\text{Bi}_2\text{Se}_3$  [83], etc., and may have a close relation to topological superconductivity. This renders  $R\text{Te}_3$  an intriguing candidate to explore topological superconductivity for future studies. Nevertheless, the pressure-induced superconductivity in  $\text{GdTe}_3$  is very unusual, and needs more theoretical and experimental inputs to clarify its origin.

#### IV. CONCLUSION

In summary, based on band structure calculations, a magnetic-field-induced topological transition from a topological trivial state to a topological Weyl state in  $\text{GdTe}_3$  has been revealed. In addition, a magnetic-field-induced Lifshitz transition is uncovered, which may come from band splitting. High-pressure electrical transport measurements reveal an unusual superconducting state with a nearly invariant

superconducting transition temperature spanning a wide range of pressure. These results suggest that  $\text{GdTe}_3$  provides a unique platform for exploring exotic physics involving CDW, magnetism, topology, and superconductivity.

#### ACKNOWLEDGMENTS

This work was supported by the Ministry of Science and Technology of China (Grant No. 2022YFA1402203), the Natural Science Foundation of China (Grant No. 12174064), and the Shanghai Municipal Science and Technology Major Project (Grant No. 2019SHZDZX01). E.J.C. acknowledges support from the Deutsche Forschungsgemeinschaft (DFG) through the project C07 of the Collaborative Research Center SFB 1143 (Project ID 247310070) and financial support from the Alexander von Humboldt Foundation. Y.F.G. was supported by the open project of Beijing National Laboratory for Condensed Matter Physics (Grant No. ZBJ2106110017) and the open project from State Key Laboratory of Surface Physics and Department of Physics, Fudan University (Grant No. KF2022\_13). J.L. acknowledges support from the Science and Technology Commission of the Shanghai Municipality (Grant No. 21JC1405100).

- 
- [1] P. Chen, J. W. Su, Z. X. Li, D. Y. Li, L. J. Pi, X. Zhou, and T. Y. Zhai, *Adv. Funct. Mater.* **31**, 2008790 (2021).
- [2] B. Huang, G. Clark, E. Navarro-Moratalla, D. R. Klein, R. Cheng, K. L. Seyler, D. Zhong, E. Schmidgall, M. A. McGuire, D. H. Cobden, W. Yao, D. Xiao, P. Jarillo-Herrero, and X. Xu, *Nature (London)* **546**, 270 (2017).
- [3] C. Gong, L. Li, Z. Li, H. Ji, A. Stern, Y. Xia, T. Cao, W. Bao, C. Wang, Y. Wang, Z. Q. Qiu, R. J. Cava, S. G. Louie, J. Xia, and X. Zhang, *Nature (London)* **546**, 265 (2017).
- [4] D. Ghazaryan, M. T. Greenaway, Z. Wang, V. H. Guarochico-Moreira, I. J. Vera-Marun, J. Yin, Y. Liao, S. V. Morozov, O. Kristanovski, A. I. Lichtenstein, M. I. Katsnelson, F. Withers, A. Mishchenko, L. Eaves, A. K. Geim, K. S. Novoselov, and A. Misra, *Nat. Electron.* **1**, 344 (2018).
- [5] M. Kim, P. Kumaravadeivel, J. Birkbeck, W. Kuang, S. G. Xu, D. G. Hopkinson, J. Knolle, P. A. McClarty, A. I. Berdyugin, M. B. Shalom, R. B. Gorbachev, S. J. Haigh, S. Liu, J. H. Edgar, K. S. Novoselov, I. V. Grigorieva, and A. K. Geim, *Nat. Electron.* **2**, 457 (2019).
- [6] J.-U. Lee, S. Lee, J. H. Ryoo, S. Kang, T. Y. Kim, P. Kim, C.-H. Park, J.-G. Park, and H. Cheong, *Nano Lett.* **16**, 7433 (2016).
- [7] T. Song, X. Cai, M. W.-Y. Tu, X. Zhang, B. Huang, N. P. Wilson, K. L. Seyler, L. Zhu, T. Taniguchi, K. Watanabe, M. A. McGuire, D. H. Cobden, D. Xiao, W. Yao, and X. Xu, *Science* **360**, 1214 (2018).
- [8] D. R. Klein, D. MacNeill, J. L. Lado, D. Soriano, E. Navarro-Moratalla, K. Watanabe, T. Taniguchi, S. Manni, P. Canfield, J. Fernández-Rossier, and P. Jarillo-Herrero, *Science* **360**, 1218 (2018).
- [9] Z. Wang, I. Gutiérrez-Lezama, N. Ubrig, M. Kroner, M. Gibertini, T. Taniguchi, K. Watanabe, A. Imamoğlu, and E. Giannini, *Nat. Commun.* **9**, 2516 (2018).
- [10] H. H. Kim, B. Yang, T. Patel, F. Sfigakis, C. Li, S. Tian, H. L. Lei, and A. W. Tsen, *Nano Lett.* **18**, 4885 (2018).
- [11] Y. J. Deng, Y. J. Yu, Y. C. Song, J. Zhang, N. Z. Wang, Z. Sun, Y. Yi, Y. Z. Wu, S. Wu, J. Zhu, J. Wang, X. H. Chen, and Y. B. Zhang, *Nature (London)* **563**, 94 (2018).
- [12] B. Huang, G. Clark, D. R. Klein, D. MacNeill, E. Navarro-Moratalla, K. L. Seyler, N. Wilson, M. A. McGuire, D. H. Cobden, D. Xiao, W. Yao, P. Jarillo-Herrero, and X. Xu, *Nat. Nanotechnol.* **13**, 544 (2018).
- [13] S. Jiang, L. Li, Z. Wang, K. F. Mak, and J. Shan, *Nat. Nanotechnol.* **13**, 549 (2018).
- [14] Z. Y. Sun, Y. F. Yi, T. C. Song, G. Clark, B. Huang, Y. W. Shan, S. Wu, D. Huang, C. L. Gao, Z. H. Chen, M. McGuire, T. Cao, D. Xiao, W. Liu, W. Yao, X. D. Xu, and S. W. Wu, *Nature (London)* **572**, 497 (2019).
- [15] L. Balents, C. R. Dean, D. K. Efetov, and A. F. Young, *Nat. Phys.* **16**, 725 (2020).
- [16] D. M. Kennes, M. Claassen, L. Xian, A. Georges, A. J. Millis, J. Hone, C. R. Dean, D. N. Basov, A. N. Pasupathy, and A. Rubio, *Nat. Phys.* **17**, 155 (2021).
- [17] H. C. Xie, X. P. Luo, G. Ye, Z. P. Ye, H. W. Ge, S. H. Sung, E. Rennich, S. H. Yan, Y. Fu, S. J. Tian, H. C. Lei, R. Hovden, K. Sun, R. He, and L. Y. Zhao, *Nat. Phys.* **18**, 30 (2022).
- [18] C.-W. Chen, J. Choe, and E. Morosan, *Rep. Prog. Phys.* **79**, 084505 (2016).
- [19] H. Watanabe, H. Chun Po, and A. Vishwanath, *Sci. Adv.* **4**, eaat8685 (2018).
- [20] J. Y. Zou, Z. R. He, and G. Xu, *npj Comput. Mater.* **5**, 96 (2019).
- [21] Y. F. Xu, L. Elcoro, Z.-D. Song, B. J. Wieder, M. G. Vergniory, N. Regnault, Y. L. Chen, C. Felser, and B. A. Bernevig, *Nature (London)* **586**, 702 (2020).
- [22] B. A. Bernevig, C. Felser, and H. Beidenkopf, *Nature (London)* **603**, 41 (2022).
- [23] N. Nagaosa, J. Sinova, S. Onoda, A. H. MacDonald, and N. P. Ong, *Rev. Mod. Phys.* **82**, 1539 (2010).

- [24] Q. Qin, L. Liu, W. N. Lin, X. Y. Shu, Q. D. Xie, Z. Lim, C. J. Li, S. K. He, G. M. Chow, and J. S. Chen, *Adv. Mater.* **31**, 1807008 (2019).
- [25] Y. Xu, L. Das, J. Z. Ma, C. J. Yi, S. M. Nie, Y. G. Shi, A. Tiwari, S. S. Tsirkin, T. Neupert, M. Medarde, M. Shi, J. Chang, and T. Shang, *Phys. Rev. Lett.* **126**, 076602 (2021).
- [26] T. Lancaster, *Contemp. Phys.* **60**, 246 (2019).
- [27] J.-Z. Ma, S. M. Nie, C. J. Yi, J. Jandke, T. Shang, M. Y. Yao, M. Naamneh, L. Q. Yan, Y. Sun, A. Chikina, V. N. Strocov, M. Medarde, M. Song, Y.-M. Xiong, G. Xu, W. Wulfhekkel, J. Mesot, M. Reticcioli, C. Franchini, C. Mudry, M. Müller, Y. G. Shi, T. Qian, H. Ding, and M. Shi, *Sci. Adv.* **5**, eaaw4718 (2019).
- [28] E. J. Cheng, W. Xia, X. B. Shi, H. W. Fang, C. W. Wang, C. Y. Xi, S. W. Xu, D. C. Peets, L. S. Wang, H. Su, L. Pi, W. Ren, X. Wang, N. Yu, Y. L. Chen, W. W. Zhao, Z. K. Liu, Y. F. Guo, and S. Y. Li, *Nat. Commun.* **12**, 6970 (2021).
- [29] H. Su, B. C. Gong, W. J. Shi, H. F. Yang, H. Y. Wang, W. Xia, Z. H. Yu, P.-J. Guo, J. H. Wang, L. C. Ding, L. C. Xu, X. K. Li, X. Wang, Z. Q. Zou, Na Yu, Z. W. Zhu, Y. L. Chen, Z. K. Liu, K. Liu, G. Li *et al.*, *APL Mater.* **8**, 011109 (2020).
- [30] J. Yuan, X. B. Shi, H. Su, X. Zhang, X. Wang, N. Yu, Z. Q. Zou, W. W. Zhao, J. P. Liu, and Y. F. Guo, *Phys. Rev. B* **106**, 054411 (2022).
- [31] S. H. Lee, D. Graf, L. J. Min, Y. Zhu, H. M. Yi, S. Ciocys, Y. X. Wang, E. S. Choi, R. Basnet, A. Fereidouni, A. Wegner, Y.-F. Zhao, K. Verlinde, J. Y. He, R. Redwing, V. Gopalan, H. O. H. Churchill, A. Lanzara, N. Samarth, C.-Z. Chang *et al.*, *Phys. Rev. X* **11**, 031032 (2021).
- [32] J. Gaudet, H.-Y. Yang, S. Baidya, B. Z. Lu, G. Y. Xu, Y. Zhao, J. A. Rodriguez-Rivera, C. M. Hoffmann, D. E. Graf, D. H. Torchinsky, P. Nikolić, D. Vanderbilt, F. Tafti, and C. L. Broholm, *Nat. Mater.* **20**, 1650 (2021).
- [33] Y. Iyeiri, T. Okumura, C. Michioka, and K. Suzuki, *Phys. Rev. B* **67**, 144417 (2003).
- [34] N. Ru, J.-H. Chu, and I. R. Fisher, *Phys. Rev. B* **78**, 012410 (2008).
- [35] A. A. Sinchenko, P. Lejay, O. Leynaud, and P. Monceau, *Solid State Commun.* **188**, 67 (2014).
- [36] J. Laverock, S. B. Dugdale, Zs. Major, M. A. Alam, N. Ru, I. R. Fisher, G. Santi, and E. Bruno, *Phys. Rev. B* **71**, 085114 (2005).
- [37] N. Ru and I. R. Fisher, *Phys. Rev. B* **73**, 033101 (2006).
- [38] K. J. Dalgaard, S. Lei, S. Wiedmann, M. Bremholm, and L. M. Schoop, *Phys. Rev. B* **102**, 245109 (2020).
- [39] J. Kopaczek, H. Li, K. Yumigeta, R. Sailus, M. Y. Sayyad, S. T. R. Moosavy, R. Kudrawiec, and S. Tongay, *J. Mater. Chem. C* **10**, 11995 (2022).
- [40] A. Sacchetti, C. L. Condrón, S. N. Gvasaliya, F. Pfúner, M. Lavagnini, M. Baldini, M. F. Toney, M. Merlini, M. Hanfland, J. Mesot, J.-H. Chu, I. R. Fisher, P. Postorino, and L. Degiorgi, *Phys. Rev. B* **79**, 201101(R) (2009).
- [41] D. A. Zocco, J. J. Hamlin, T. A. Sayles, M. B. Maple, J.-H. Chu, and I. R. Fisher, *Phys. Rev. B* **79**, 134428 (2009).
- [42] A. Sacchetti, E. Arcangeletti, A. Perucchi, L. Baldassarre, P. Postorino, S. Lupi, N. Ru, I. R. Fisher, and L. Degiorgi, *Phys. Rev. Lett.* **98**, 026401 (2007).
- [43] D. A. Zocco, J. J. Hamlin, K. Grube, J.-H. Chu, H.-H. Kuo, I. R. Fisher, and M. B. Maple, *Phys. Rev. B* **91**, 205114 (2015).
- [44] A. Banerjee, Y. Feng, D. M. Silevitch, J. Wang, J. C. Lang, H.-H. Kuo, I. R. Fisher, and T. F. Rosenbaum, *Phys. Rev. B* **87**, 155131 (2013).
- [45] R. Y. Chen, B. F. Hu, T. Dong, and N. L. Wang, *Phys. Rev. B* **89**, 075114 (2014).
- [46] A. A. Sinchenko, P. D. Grigoriev, P. Monceau, P. Lejay, and V. N. Zverev, *J. Low Temp. Phys.* **185**, 657 (2016).
- [47] S. M. Lei, J. J. Lin, Y. Y. Jia, M. Gray, A. Topp, G. Farahi, S. Klemenž, T. Gao, F. Rodolakis, J. L. McChesney, C. R. Ast, A. Yazdani, K. S. Burch, S. F. Wu, N. P. Ong, and L. M. Schoop, *Sci. Adv.* **6**, eaay6407 (2020).
- [48] Y. P. Wang, I. Petrides, G. McNamara, M. M. Hosen, S. M. Lei, Y.-C. Wu, J. L. Hart, H. Y. Lv, J. Yan, D. Xiao, J. J. Cha, P. Narang, L. M. Schoop, and K. S. Burch, *Nature (London)* **606**, 896 (2022).
- [49] Z. Xu, S.-H. Ji, L. Tang, J. Wu, N. Li, X. Cai, and X. Chen, *Chin. Phys. Lett.* **38**, 077102 (2021).
- [50] Q. Guo, D. Bao, L. J. Zhao, and S. Ebusu, *Phys. B: Condens. Matter* **617**, 413153 (2021).
- [51] H. K. Mao, J. Xu, and P. M. Bell, *J. Geophys. Res.* **91**, 4673 (1986).
- [52] G. Kresse and J. Furthmüller, *Comput. Mater. Sci.* **6**, 15 (1996).
- [53] G. Kresse and J. Furthmüller, *Phys. Rev. B* **54**, 11169 (1996).
- [54] S. D. Chakarova-Käck, E. Schröder, B. I. Lundqvist, and D. C. Langreth, *Phys. Rev. Lett.* **96**, 146107 (2006).
- [55] J. Klimeš, D. R. Bowler, and A. Michaelides, *Phys. Rev. B* **83**, 195131 (2011).
- [56] S. Grimme, S. Ehrlich, and L. Goerigk, *J. Comput. Chem.* **32**, 1456 (2011).
- [57] A. A. Mostofi, J. R. Yates, Y.-S. Lee, I. Souza, D. Vanderbilt, and N. Marzari, *Comput. Phys. Commun.* **178**, 685 (2008).
- [58] N. Marzari and D. Vanderbilt, *Phys. Rev. B* **56**, 12847 (1997).
- [59] I. Souza, N. Marzari, and D. Vanderbilt, *Phys. Rev. B* **65**, 035109 (2001).
- [60] Q. S. Wu, S. N. Zhang, H.-F. Song, M. Troyer, and A. A. Soluyanov, *Comput. Phys. Commun.* **224**, 405 (2018).
- [61] E. J. Cheng, W. Xia, X. B. Shi, Z. H. Yu, L. Wang, L. M. Yan, D. C. Peets, C. C. Zhu, H. Su, Y. Zhang, D. Z. Dai, X. Wang, Z. Q. Zou, N. Yu, X. F. Kou, W. G. Yang, W. W. Zhao, Y. F. Guo, and S. Y. Li, *npj Quantum Mater.* **5**, 38 (2020).
- [62] E. J. Cheng, X. B. Shi, L. M. Yan, T. H. Huang, F. L. Liu, W. L. Ma, Z. J. Wang, S. Jia, J. Sun, W. W. Zhao, W. G. Yang, Y. Xu, and S. Y. Li, *npj Quantum Mater.* **7**, 93 (2022).
- [63] Q. Q. Zeng, H. Y. Sun, J. L. Shen, Q. S. Yao, Q. Zhang, N. N. Li, L. Jiao, H. X. Wei, C. Felser, Y. G. Wang, Q. H. Liu, and E. K. Liu, *Adv. Quantum Technol.* **5**, 2100149 (2022).
- [64] E. J. Cheng, D. C. Peets, C. Y. Xi, Y. Y. Huang, L. Pi, and S. Y. Li, *Phys. Rev. B* **100**, 054509 (2019).
- [65] N. Ru, R. A. Borzi, A. Rost, A. P. Mackenzie, J. Laverock, S. B. Dugdale, and I. R. Fisher, *Phys. Rev. B* **78**, 045123 (2008).
- [66] H. K. Mao, X. J. Chen, Y. Ding, B. Li, and L. Wang, *Rev. Mod. Phys.* **90**, 015007 (2018).
- [67] B. F. Hu, P. Zheng, R. H. Yuan, T. Dong, B. Cheng, Z. G. Chen, and N. L. Wang, *Phys. Rev. B* **83**, 155113 (2011).
- [68] B. F. Hu, B. Cheng, R. H. Yuan, T. Dong, and N. L. Wang, *Phys. Rev. B* **90**, 085105 (2014).
- [69] E. DiMasi, M. C. Aronson, J. F. Mansfield, B. Foran, and S. Lee, *Phys. Rev. B* **52**, 14516 (1995).
- [70] C. D. Malliakas and M. G. Kanatzidis, *J. Am. Chem. Soc.* **128**, 12612 (2006).

- [71] R. G. Moore, V. Brouet, R. He, D. H. Lu, N. Ru, J.-H. Chu, I. R. Fisher, and Z.-X. Shen, *Phys. Rev. B* **81**, 073102 (2010).
- [72] N. Ru, C. L. Condon, G. Y. Margulis, K. Y. Shin, J. Laverock, S. B. Dugdale, M. F. Toney, and I. R. Fisher, *Phys. Rev. B* **77**, 035114 (2008).
- [73] J. S. Liu, S. C. Huan, Z. H. Liu, W. L. Liu, Z. T. Liu, X. L. Lu, Z. Huang, Z. C. Jiang, X. Wang, N. Yu, Z. Q. Zou, Y. F. Guo, and D. W. Shen, *Phys. Rev. Mater.* **4**, 114005 (2020).
- [74] F. P. Bundy and K. J. Dunn, *Phys. Rev. Lett.* **44**, 1623 (1980).
- [75] Y. Akahama, M. Kobayashi, and H. Kawamura, *Solid State Commun.* **84**, 803 (1992).
- [76] Z. F. Weng, M. Smidman, L. Jiao, X. Lu, and H. Q. Yuan, *Rep. Prog. Phys.* **79**, 094503 (2016).
- [77] M. Maschek, S. Rosenkranz, R. Heid, A. H. Said, P. Giraldo-Gallo, I. R. Fisher, and F. Weber, *Phys. Rev. B* **91**, 235146 (2015).
- [78] N. Lazarević, Z. V. Popović, R. Hu, and C. Petrovic, *Phys. Rev. B* **83**, 024302 (2011).
- [79] M. D. Johannes and I. I. Mazin, *Phys. Rev. B* **77**, 165135 (2008).
- [80] H.-M. Eiter, M. Lavagnini, R. Hackl, E. A. Nowadnick, A. F. Kemper, T. P. Devereaux, J.-H. Chu, J. G. Analytis, I. R. Fisher, and L. Degiorgi, *Proc. Natl. Acad. Sci. USA* **110**, 64 (2013).
- [81] K. Terashima, Y. Sekiba, J. H. Bowen, K. Nakayama, T. Kawahara, T. Satob, P. Richard, Y.-M. Xu, L. J. Li, G. H. Cao, Z.-A. Xu, H. Ding, and T. Takahashi, *Proc. Natl. Acad. Sci. USA* **106**, 7330 (2009).
- [82] L. P. He, Y. T. Jia, S. J. Zhang, X. C. Hong, C. Q. Jin, and S. Y. Li, *npj Quantum Mater.* **1**, 16014 (2016).
- [83] K. Kirshenbaum, P. S. Syers, A. P. Hope, N. P. Butch, J. R. Jeffries, S. T. Weir, J. J. Hamlin, M. B. Maple, Y. K. Vohra, and J. Paglione, *Phys. Rev. Lett.* **111**, 087001 (2013).